AIP Applied Physics Letters

Observation of enhanced carrier transport properties of Si 100-oriented whiskers under uniaxial strains

Kun Zheng, Ruiwen Shao, Qingsong Deng, Yuefei Zhang, Yujie Li, Xiaodong Han, Ze Zhang, and Jin Zou

Citation: Applied Physics Letters **104**, 013111 (2014); doi: 10.1063/1.4861425
View online: http://dx.doi.org/10.1063/1.4861425
View Table of Contents: http://scitation.aip.org/content/aip/journal/apl/104/1?ver=pdfcov
Published by the AIP Publishing

Observation of enhanced carrier transport properties of Si ⟨100⟩-oriented whiskers under uniaxial strains

Kun Zheng,[1,a)] Ruiwen Shao,[1] Qingsong Deng,[1] Yuefei Zhang,[1] Yujie Li,[1] Xiaodong Han,[1] Ze Zhang,[2] and Jin Zou[3,a)]
[1]*Institute of Microstructure and Properties of Advanced Materials, Beijing University of Technology, Beijing 100124, China*
[2]*Department of Materials Science, Zhejiang University, Hangzhou, Zhejiang 310058, China*
[3]*Material Engineering and Centre for Microscopy and Microanalysis, The University of Queensland, Brisbane, Queensland 4072, Australia*

(Received 7 August 2013; accepted 21 December 2013; published online 9 January 2014)

In this study, enhancements of the carrier transport properties of p-type ⟨100⟩-oriented Si whiskers are observed under uniaxial tensile and compressive strains. It has been found that over 400% enhancement of electrical conductivity is achieved under a 2% tensile strain, while a 2% compressive strain can only cause ~80% conductivity enhancement. The enhancements are mainly attributed to the breaking of the degeneracy of the *v*2 and *v*1 valence bands induced a reduction of the hole effective mass. This study provides an important insight of how the carrier mobility variation caused by the strain impact on their transport properties. © *2014 AIP Publishing LLC*. [http://dx.doi.org/10.1063/1.4861425]

Si is a primary semiconductor that has been widely used in microelectronics due to its nature of indirect band gap.[1] Since elastic strain changes the atomic distance of a material, its electronic band structure can be manipulated under an elastic strain, resulting in an alternation in its physical properties. This feature has been used to enhance the carrier mobility in strained-Si complementary metal oxide semiconductors,[2] making convenient for human's life in foldable and flexible devices,[3,4] sensors,[5] nano-generators,[6] and so on. For low-dimensional materials, the effect of strain on tuning physical properties becomes enhanced when compared with their bulk counterparts owing to the broader tunable range resulted from the large elasticity when the dimension of a material is scaled down.[7–12] For example, the loadable elastic strain of nanomaterials can be approximately reached to their theoretical values,[13–20] which can be increased by 2–3 orders of magnitude higher than their bulk forms. Thus, such a huge difference for the loadable strain between the nanomaterials and their bulk counterparts may bring remarkable changes in physical properties.[7,11]

For Si, efforts have been paid to alter the carrier transport properties induced by strain in order to find highly sensitive strain gauges or a more effective mode to enhance the carrier mobility by theoretical calculations[21–31] or experiments.[32–38] It has been well demonstrated that the orientation, size, doping type, and level as well as the strain state are the primary factors[22,26,30,31] affecting the band structure, carrier effective mass, and electric properties for strained crystalline Si. In terms of directional considerations, the ⟨100⟩, ⟨110⟩, and ⟨111⟩ are the most important directions for the electrical transport properties of strained Si (particular one-dimensional Si) in practical applications or theoretical investigations. Interestingly, the electrical transport properties of strained ⟨111⟩ and ⟨110⟩ oriented one-dimensional Si nanostructures have been studied experimentally,[33–38] while very few reported on the understanding of the strained ⟨100⟩ orientated Si through experiments.[39] The current understanding of the electrical transport properties of strained ⟨100⟩-oriented Si was limited by theoretical considerations.[24,27,29–31] It is necessary and important to clarify the carrier transport properties of strained ⟨100⟩-oriented one-dimensional Si experimentally. Here, through our *in-situ* uniaxial tension and compression experiments on p-type ⟨100⟩-oriented Si whiskers in a transmission electron microscope (TEM), the strain effects on electrical transport properties along the ⟨100⟩ direction of single crystalline Si whiskers were studied. It has been found that both strain modes can improve the conductivity of p-type ⟨100⟩-oriented Si, while the tension is more effective than compression. The physical reason behind this extraordinary finding was clarified.

A p-type doped Si ⟨001⟩ film with the electrical resistance of $14 \sim 22\Omega \cdot \mathrm{cm}$ and with a lateral dimension of $1\,\mathrm{mm} \times 100\,\mu\mathrm{m}$ (with side edges of {100} facets) and a thickness of 300 nm was used to prepare Si ⟨100⟩-oriented whiskers using focus ion beam (FIB) technology. The fabricated Si ⟨100⟩-oriented whiskers have a lateral dimension of several hundred nm, which were deformed in a scanning tunnelling microscope (STM)-TEM electrical probing system (Nanofactory Instruments AB) inside a JEOL-2010 TEM, in which a fresh tungsten tip was placed on movable terminal of the STM holder, and the Si whiskers were placed on fixed part of the probing system. The tungsten tip can be precisely controlled by the commercial software and electronics in three-dimensional that can approach, contact, and manipulate the sample. Simultaneously, the corresponding *I-V* curves of deformed whiskers can be recorded.

Figure 1(a) is a schematic illustration of the experiment setup, in which four whiskers were drawn with two straight whiskers and two with their "head" having a hole in the middle. Such a design allows the compressive test to be performed on the straight whiskers, while the tensile tests to be

a)Authors to whom correspondence should be addressed. Electronic addresses: kunzheng@bjut.edu.cn and j.zou@uq.edu.au

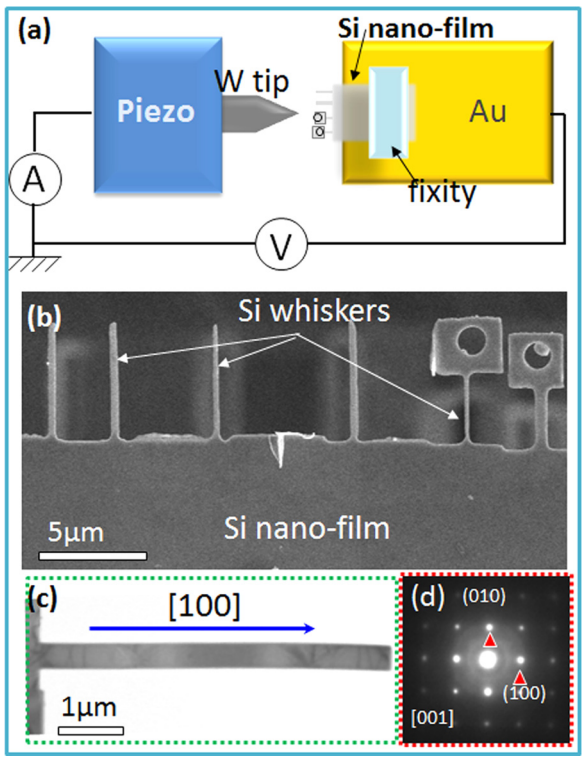

FIG. 1. (a) Schematic of experimental setup. (b) SEM of Si whiskers fabricated from Si film by FIB. (c) TEM image of a single Si whisker. (d) SAED pattern of the Si whisker showing ⟨100⟩ being the axial direction.

performed on the whiskers with "head" (in this case, the hook-shaped tungsten tip will used to pull the "head"). Figure 1(b) is a scanning electron microscopy (SEM) image and shows several FIB prepared Si ⟨100⟩-orientation whiskers, in which a couple of "heads" on top of whiskers can be seen. Figure 1(c) is a TEM image of a typical Si whisker and Fig. 1(d) is the corresponding selected area electron diffraction (SAED) pattern, from which the axial direction of the Si whisker can be confirmed to be along a ⟨100⟩ direction. By applying the uniaxial tensile and compressive strains on the Si whiskers, different *I-V* curves were obtained. By correlating the experimentally measured electrical behaviour of our p-type Si ⟨100⟩-oriented whiskers with the reported theoretical calculations, their intrinsic electrical transport properties are clarified.

Figure 2(a) shows a set of TEM images that record the length change of the Si whisker during different tensile strain realized by the pull of the "head" using a hook-shape tungsten tip. The length of Si whisker can be measured by the Gatan DigitalMicrograph software (version version 1.84.1282). Although the accuracy of measured length of any nanostructures using this software may vary with the imaging condition, the relevant length change, and, in turn, the corresponding tensile strain, can be accurately determined by comparing the change of the measured lengths during the deformation. Under this consideration, the initial length of the Si whisker was measured as 6.377 μm. (state 1, note that this value is not necessary to be the accurate length of the Si whisker) without the hooking the "head" by the hook-shaped tungsten tip. At the beginning of the tensile experiment, the tungsten tip was hooked with the head and pull slightly, but ensuring the whisker length to maintain as 6.377 μm (state 2), identical to the initial length. Then a series of pulling were performed that results in measured lengths of 6.417 μm (state 3), 6.456 μm (state 4), 6.476 μm (state 5), 6.515 μm (state 6), and 6.535 μm (state 7), respectively, which in turn correspond to tensile strains of 0.63%, 1.24%, 1.55%, 2.16%, and 2.48%, respectively. The pulling was continued until a crack is generated (state 8). At that time, the strain reduced to 0.93% (length: 6.436 μm). For each pull, an *I-V* curve was recorded, in which, a voltage sweep from −5000 mV to +5000 mV was applied. Figure 2(b) shows *I-V* curves measured under different tensile strains. As can be seen, with increasing the tensile strain, the electrical conductivity increases. In the strain-free case, the *I-V* curve (the black curve) indicates the intrinsic electrical property, so that the increase in I with increasing V is caused by the increased carrier density and mobility. When a uniaxial tensile strain is applied to the Si whisker, enhanced electrical conductivities can be witnessed with, under a given V, the higher the applied uniaxial tensile strain, the higher the I (refer to the dashed arrow). It should be mentioned that, under such two-terminal *I-V* measurement setup, the measured data should reflect the combination of the resistances of Si whisker and its underlying Si film (refer to Figure 1(b)). Therefore, it is necessary to estimate the resistance contribution coming from the Si whisker alone. It is well known that, for a material, the resistance R can be expressed as $R = \rho \cdot l/s = \rho \cdot l/(w \cdot t)$, where ρ is the resistivity; l is the length; s is the product of width (w) and thickness (t). For the Si whisker and the film, they have the same ρ and t, so that $R_{whisker}/R_{film} = l_{whisker} \cdot w_{film}/l_{film} \cdot w_{whisker}$. In this experiment, $l_{whisker}$ and l_{film} can be, respectively, measured as 6 μm and 30 μm; and $w_{whisker}$ *and* w_{film} as ∼0.3 μm and ∼100 μm, respectively, leading to $R_{whisker}/R_{film} \approx 60$. In addition, the Si film can be considered as a rigid under the external stress, so that the variation of the measured conductivity of the Si film can be neglected. In addition, the variation of conductivity induced by the change of contact between the tungsten tip and the Si whisker has also been evaluated, which can also been neglected. Accordingly, the obtained enhanced electrical conductivities should be primarily contributed from the increased electrical conductivity of the Si whisker when the uniaxial tensile stress is increased.

Similarly, we also measure the electrical properties of p-type Si ⟨100⟩ whiskers under the compressive strain. In this experiment, we use tungsten tips with flat ends to punch Si whiskers. Similar to the measurement of tensile experiment, the TEM images can be recorded under different compressive strain, and Figure 3(a) shows such a set of TEM images taken from a typical Si whisker. The initial length of this Si whisker can be measured as 1.886 μm with a width of 380 nm. Though controlling the tip's movement, the compressive strain can be applied to this whisker. A series of strains can then be obtained, namely, 0.67% (state 2), 1.11% (state 3), 2.23% (state 4), 2.68% (state 5), 3.57% (state 6), 5.13% (state 7), and 6.7% (state 8), respectively. Different from the tensile deformation mode, the compressive strain may induce bending or buckling deformations for one-dimensional nanostructures,[40] so that care must be taken to avoid these kinds of unwanted deformations in order to gain true compression data. There are two approaches to avoid

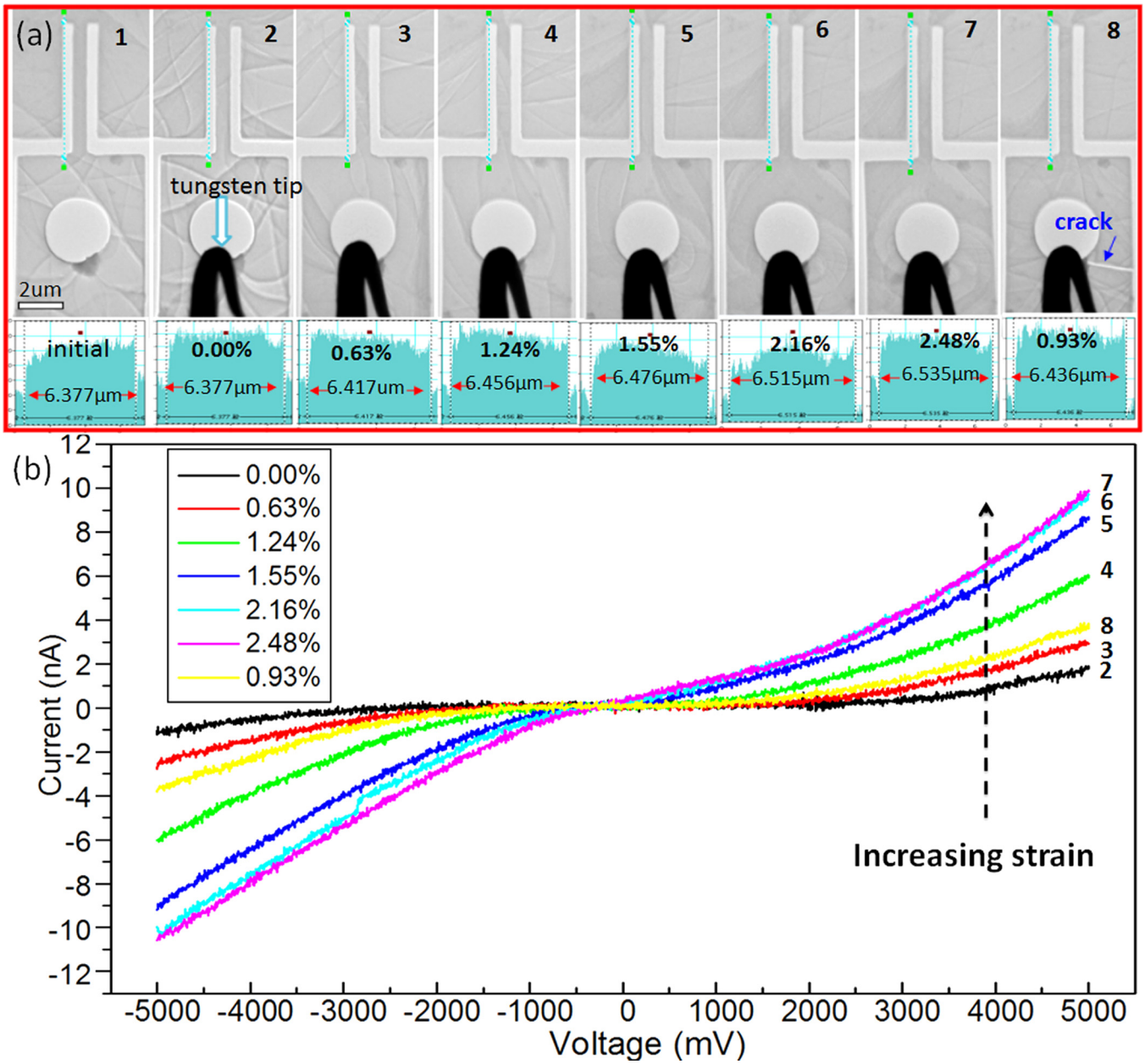

FIG. 2. The electrical measurement of tensile process of an individual Si whisker. (a) Sequential images of a tensile Si whisker: "1" is a free state, "2" shows a tungsten tip just hooked this whisker through the hole, "2"–"8" show different states with different strains, "8" indicates a reduction of tensile strain due to the formation of a crack. (b) A series of I-V curves under different strains corresponding to the states "2"–"8." As can be seen, the conductivity is enhanced with increasing uniaxial tensile strain.

them:[41] reducing their aspect ratio and employing a uniaxial compressive stress. In this compressive experiment, the aspect ratio is 5, so that the possibility of causing buckling deformation is reduced substantially. From the TEM investigations, bending or buckling was not observed. As a consequence, the measured compressive strains should reflect the true nature. Figure 3(b) is the simultaneously measured corresponding *I-V* curves. Similar to the case of uniaxial tensile process, the enhancement of electrical conductivities with increasing the compressive strain is observed.

To understand the obtained *I-V* curves under different strains (compressive and tensile) and to clarify the relationship of measured electrical properties and loaded strain, the relative changes in measured electric current ($\Delta I/I_0$) at 5000 mV are plotted as a function of the strain, in which I_0 is the initial electric current at 5000 mV of the strain-free Si whiskers. Figure 4 shows such a plot. Although the data are not taken from one whisker, but the two whiskers were cut from a piece of Si film, so that they should have the same characteristics, such as carrier density and mobility. It is of interest to note that the $\Delta I/I_0$ increases with increasing the strain (both compressive and tensile). Nevertheless, such an increase shows different behaviours under the compressive and tensile strains. Under the tensile strain, $\Delta I/I_0$ increases sharply from the strain-free up to ~2%, beyond that, $\Delta I/I_0$ has a modest increase. On the other hand, under the compressive strain, $\Delta I/I_0$ increases almost linearly with the compressive strain up to 6% and even beyond. Furthermore, at the strain level of 2%, ~400% change in the electrical current can be found under the tensile strain, while only ~80% change in the electrical current can be seen under the

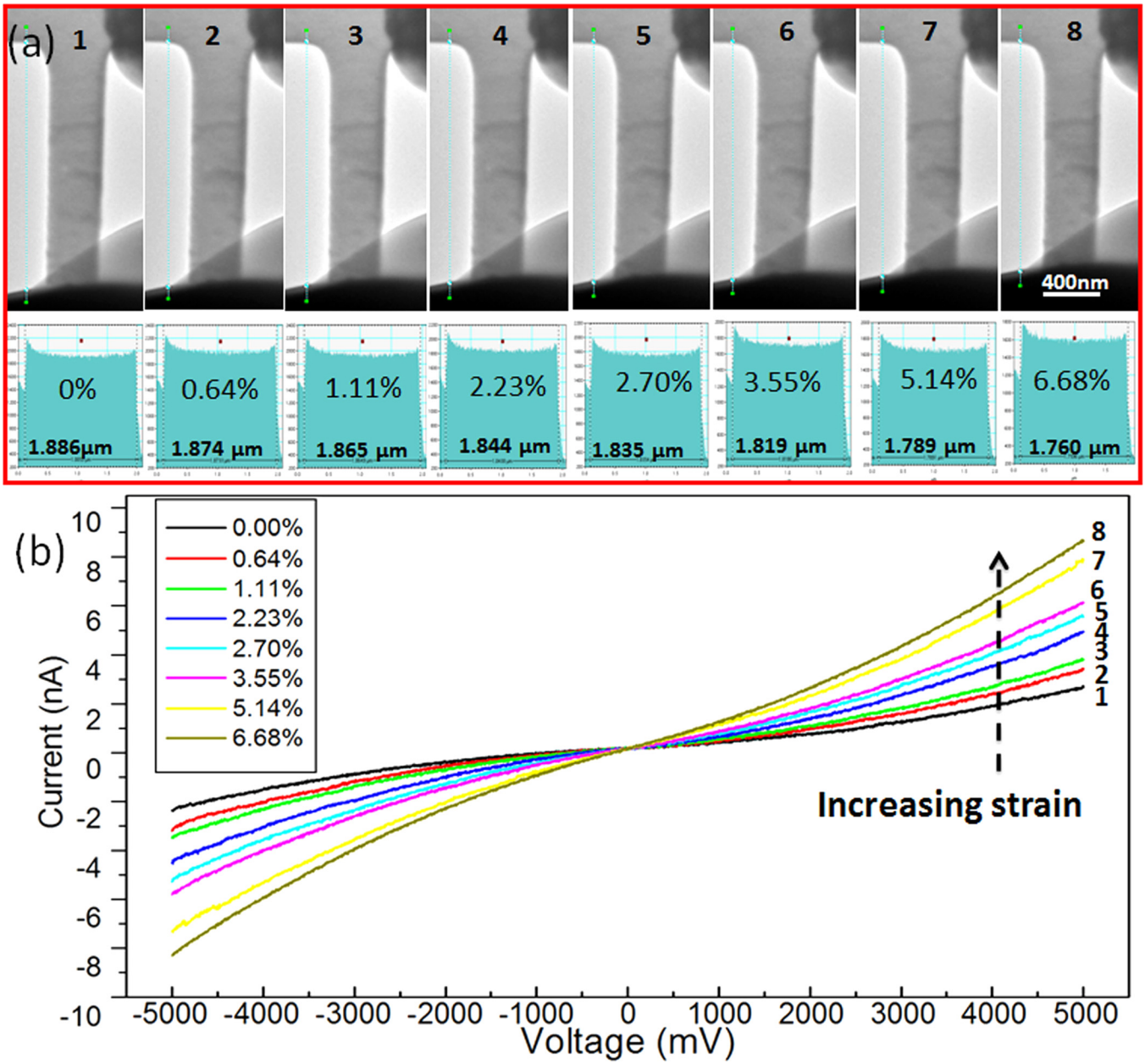

FIG. 3. The electrical measurement of compressive process of an individual Si whisker. (a) Sequential images of a compressive Si whisker: "1" shows another flat tungsten tip just contacted with this whisker, "2"–"8" show different states with different strains, (b) a series of I-V curves under different strains corresponding to the states "1"–"8." As can be seen, the conductivity is also enhanced with increasing uniaxial compressive strain.

compressive strain. To understand this observed conductive behaviour, we need to understand the physics behind these trends. It is well known that strain can induce the band structure modulation and change transport properties. For Si, the change of transport properties is mainly attributed to the variation of carrier mobility.[27,28,33,34] Carrier mobility depends upon two aspects: transport effect mass and the intervalley scattering. Leu *et al.*[28] calculated the band structure of strained bulk Si using nonlocal empirical pseudo-potentials. Under the consideration of transport effect mass and the intervalley scattering, they revealed the change of electron/-hole mobility with the applied strain. Their results show that the hole mobility along the [001] direction would be enhanced with increasing both the uniaxial tensile and compressive strains, but a larger enhancement can be achieved by uniaxial tensile strain. This tendency fits well with our experimental results (in our experiments, the dominated carrier is the hole due to the p-type Si whiskers). Indeed, the main causes of the enhancement of the hole mobility are the breaking of the degeneracy of the $v2$ (heavy hole) and $v1$(light-hole) valence bands at Γ and the reduction of the transport effective mass.

In summary, we performed an *in-situ* manipulation and electrical transport measurements on individual p-type Si $\langle 100 \rangle$ whiskers using a piezo-driven STM-TEM probing system inside a TEM. It has been found that both tensile and compressive strains lead to enhanced transport properties, but their enhancements are different. It has been found that, under ~2% strain, over 400% conductivity enhancement can be achieved under the tensile strain, while only ~80% enhancement is seen for the compressive strain, suggesting that the tensile strain can significant enhance the electrical

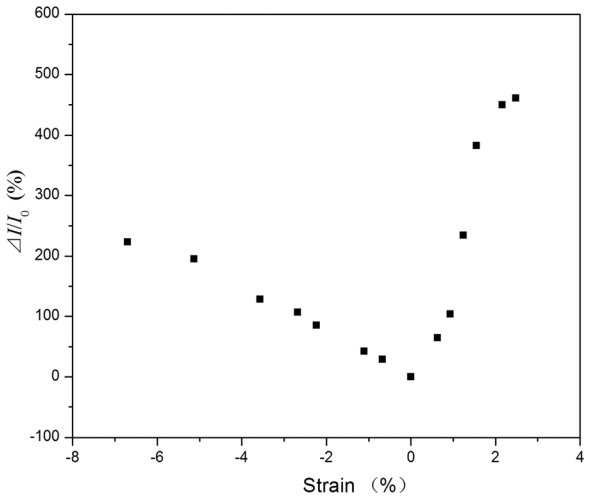

FIG. 4. Relative changes in measured electrical currents $\Delta I/I_0$ as a function of strain (compressive and tensile).

property of p-type ⟨100⟩-orientated Si whiskers. This study provides an important insight of how the carrier mobility variation caused by the strain impact on their transport properties.

This work was supported by the National Natural Science Foundation of China (11004004,11374029), the Beijing Municipal Natural Science Foundation (1112004), Beijing Nova Program (Z121103002512017, 2010B008), A Foundation for the Author of National Excellent Doctoral Dissertation of PR China, the Key Project of C-NSF (11234011) and (50831001), the National 973 Program of China (2009CB623700), and Australian Research Council.

[1]M. Chu, Y. Sun, U. Aghoram, and S. E. Tompson, Annu. Rev. Mater. Res. **39**, 203 (2009).
[2]M. Chu, Y. K. Sun, U. Aghoram, and S. E. Thompson, Annu. Rev. Mater. Res. **39**, 203 (2009).
[3]D. H. Kim, N. S. Lu, R. Ma, Y. S. Kim, R. H. Kim, S. D. Wang, J. Wu, S. M. Won, H. Tao, A. Islam *et al*., Science **333**, 838 (2011).
[4]D. H. Kim, J. H. Ahn, W. M. Choi, H. S. Kim, T. H. Kim, J. Z. Song, Y. G. Huang, Z. Liu, C. Lu, and J. A. Rogers, Science **320**, 507 (2008).
[5]C. Y. Pang, G. Y. Lee, T. Kim, S. M. Kim, H. N. Kim, S. H. Ahn, and K. Y. Suh, Nature Mater. **11**, 795 (2012).
[6]Z. L. Wang and J. H. Song, Science **312**, 242 (2006).
[7]B. Wei, K. Zheng, Y. Ji, Y. F. Zhang, Z. Zhang, and X. D. Han, Nano Lett. **12**, 4595 (2012).
[8]X. B. Han, L. Z. Kou, X. L. Lang, J. B. Xia, N. Wang, R. Qin, J. Lu, J. Xu, Z. M. Liao, X. Z. Zhang, X. D. Shan, X. F. Song, J. Y. Gao, W. L. Guo, and D. P. Yu, Adv. Mater. **21**, 4937 (2009).
[9]X. B. Han, L. Z. Kou, Z. H. Zhang, Z. Y. Zhang, X. L. Zhu, J. Xu, Z. M. Liao, W. L. Guo, and D. P. Yu, Adv. Mater. **24**, 4707 (2012).
[10]S. G. Xu, W. H. Guo, S. W. Du, M. M. T. Loy, and N. Wang, Nano Lett. **12**, 5802 (2012).
[11]G. Signorello, S. Karg, M. T. Björk, B. Gotsmann, and H. Riel, Nano Lett. **13**, 917 (2013).
[12]R. W. Shao, K. Zheng, Y. F. Zhang, Y. J. Li, Z. Zhang, and X. D. Han, Appl. Phys. Lett. **101**, 233109 (2012).
[13]G. Stan, S. Krylyuk, A. V. Davydov, I. Levin, and R. F. Cook, Nano Lett. **12**, 2599 (2012).
[14]L. Tian, Y. Q. Cheng, Z. W. Shan, J. Li, C. C. Wang, X. D. Han, J. Sun, and E. Ma, Nat. Commun. **3**, 609 (2012).
[15]Q. S. Deng, Y. Q. Cheng, Y. H. Yue, L. Zhang, Z. Zhang, X. D. Han, and E. Ma, Acta Mater. **59**, 6511 (2011).
[16]K. Zheng, X. D. Han, L. H. Wang, Y. H. Yue, Y. Qin, Y. F. Zhang, X. N. Zhang, and Z. Zhang, Nano Lett. **9**, 2471 (2009).
[17]Y. H. Yue, P. Liu, Z. Zhang, X. D. Han, and E. Ma, Nano Lett. **11**, 3151 (2011).
[18]L. H. Wang, P. Liu, P. F. Guan, M. J. Yang, J. L. Sun, Y. Q. Cheng, A. Hirata, Z. Zhang, E. Ma, M. W. Chen, and X. D. Han, Nat. Commun. **4**, 2413 (2013).
[19]L. H. Wang, Z. Zhang, and X. D. Han, NPG Asia Mater. **5**, e40 (2013).
[20]L. H. Wang, K. Zheng, Z. Zhang, and X. D. Han, Nano Lett. **11**, 2382 (2011).
[21]J. Wang, A. Rahman, A. Ghosh, G. Klimeck, and M. Lundstrom, Appl. Phys. Lett. **86**, 093113 (2005).
[22]K. Hong, J. Kim, S. Lee, and J. K. Shin, Nano Lett. **8**, 1335 (2008).
[23]K. Shiri, Y. Kong, A. Buin, and M. P. Anantram, Appl. Phys. Lett. **93**, 073114 (2008).
[24]R. N. Sajjad and K. Alam, J. Appl. Phys. **105**, 044307 (2009).
[25]T. Maegawa, T. Yamauchi, T. Hara, H. Tsuchiya, and M. Ogawa, IEEE Trans. Electron Devices **56**, 553 (2009).
[26]J. Zhang, Q. Huang, H. Yu, and S. Lei, Sensor **9**, 2746 (2009).
[27]J. X. Cao, X. G. Gong, and R. Q. Wu, Phys. Rev. B **75**, 233302 (2007).
[28]P. W. Leu, A. Svizhenko, and K. Cho, Phys. Rev. B **77**, 235305 (2008).
[29]K. Nakamura, Y. Isono, and T. Toriyama, Jpn. J. Appl. Phys. Part 1 **47**, 5132 (2008).
[30]Y. M. Niquet, C. Delerue, and C. Krzeminski, Nano Lett. **12**, 3545 (2012).
[31]M. V. Fishchetti and S. E. Laux, J. Appl. Phys. **80**, 2234 (1996).
[32]S. F. Feste, J. Knoch, S. Habicht, D. Buca, Q. T. Zhao, and S. Mantl, Solid-State Electron. **53**, 1257(2009).
[33]T. Toriyama, D. Funai, and S. Sugiyama, J. Appl. Phys. **93**, 561(2003).
[34]Y. L. Yang and X. X. Li, Nanotechnology **22**, 015501(2011).
[35]P. Neuzil, C. C. Wong, and J. Rebound, Nano Lett. **10**, 1248 (2010).
[36]A. Lugstein, M. Steinmair, A. Steiger, H. Kosina, and E. Bertagnolli, Nano Lett. **10**, 3204 (2010).
[37]R. H. He and P. D. Yang, Nat. Nanotechnol. **1**, 42 (2006).
[38]J. S. Milne, A. C. H. Rowe, S. Arscott, and C. Renner, Phys. Rev. Lett. **105**, 226802 (2010).
[39]R. Rurali, Rev. Mod. Phys. **82**, 427 (2010).
[40]C. L. Hsin, W. J. Mai, Y. D. Gu, Y. F. Gao, C. T. Huang, Y. Z. Liu, L. J. Chen, and Z. L. Wang, Adv. Mater. **20**, 3919 (2008).
[41]F. Östlund, K. Rzepiejewska-Malyska, K. Leifer, L. M. Hale, Y. Y. Tang, R. Ballarini, W. W. Gerberich, and J. Michler, Adv. Funct. Mater. **19**, 2439 (2009).